Correlation of optical and structural properties of GaN/AlN core-shell nanowires

L. Rigutti,[1,*] G. Jacopin,[1] L. Largeau,[2] E. Galopin,[2] A. De Luna Bugallo,[1] F. H. Julien,[1] J.-C. Harmand,[2] F. Glas,[2] and M. Tchernycheva[1]

[1]*Institut d'Electronique Fondamentale, Université Paris Sud XI, UMR 8622 CNRS, F-91405 Orsay, France*

[2]*Laboratoire de Photonique et Nanostructures, UPR 20 CNRS, Route de Nozay, F-91460 Marcoussis, France*

(Received 22 December 2010; revised manuscript received 10 March 2011; published 21 April 2011)

We analyze the correlation between the structural and optical properties of GaN/AlN coherent core-shell nanowire heterostructures, with different AlN shell thicknesses. The presence of an AlN shell induces a nearly uniaxial compressive strain in the core ε_{zz}^{c} oriented along the nanowire axis, which translates into a blueshift of the photoluminescence. The dependence of the photoluminescence shift on the uniaxial strain is experimentally established on the basis of correlated microphotoluminescence and high-resolution scanning transmission electron microscopy on a large number of single nanowires. The results confirm the crossing of X_A and X_C exciton energies at $\varepsilon_{zz}^{c} = 0.35\% - 0.5\%$, with a shell-to-core volume ratio $V_{\mathrm{AlN}}/V_{\mathrm{GaN}}$=0.1–0.15, as predicted by the elastic theory for purely uniaxial strain.

DOI: 10.1103/PhysRevB.83.155320 PACS number(s): 78.67.Uh, 78.55.Et, 78.66.Fd, 61.46.Km

I. INTRODUCTION

Core-shell nanowires (NWs) represent an important class of semiconductor nanostructures giving rise to numerous optoelectronic applications, such as NW light-emitting diodes and lasers,[1,2] solar cells,[3] high-current battery electrodes,[4] etc. The shell can significantly impact the structural, electrical, and optical properties of the nanowire core. For example, core-shell structures have been used to passivate the free NW surface in order to increase the carrier mobility[5] or to enhance the core luminescence intensity.[6,7]

The strain state in coherent core-shell systems has been studied by a variety of authors in the case of macroscopic structures made of materials with transverse isotropy of stiffness[8] and in nanowire heterostructures with coherent interface when their length significantly exceeds their radius.[9–13] In particular, Grønqvist *et al*. calculated by the valence force field (VFF) method and finite-element method the strain state in coherent core-shell nanowires of cylindrical and hexagonal cross sections and with cubic crystal symmetry.[12] The VFF method has also been applied to hexagonal crystals,[14] and employed for the interpretation of their experiments by Hestroffer *et al*.[13], dealing with Raman, x-ray diffraction (XRD), and high-resolution scanning transmission electron microscopy (HRSTEM) measurements on GaN/AlN core-shell heterostructures with the nanowire axis coinciding with the crystal [0001] z axis. According to these results, the strain state in a coherent core-shell heterostructure is mainly determined by the component ε_{zz} along the nanowire axis, which is uniform within the core and in the shell. This quantity is negative in the compressively strained GaN core and positive in the tensile-strained AlN shell. The strain component ε_{zz} can be well approximated by an analytic function of the volumetric ratio of core and shell, the GaN core being progressively more compressed with increasing AlN shell thickness.[13] The contribution of the in-plane component is much lower, $\varepsilon_{xx} + \varepsilon_{yy} \ll \varepsilon_{zz}$; therefore as a good approximation the strain can be considered as purely uniaxial.[12,13] The situation is thus radically different than when applying an external uniaxial stress to bulk crystals. In this latter case the uniaxial compression along one main crystal axis also implies a non-negligible tension in the perpendicular plane, proportional to the Poisson ratio of the crystal.

The effect of purely uniaxial strain along the c axis on the optical properties of GaN has never been studied experimentally in the literature. The elastic theory applied to the $\mathbf{k}\cdot\mathbf{p}$ approximation predicts that the increase of the compressive strain $|\varepsilon_{zz}|$ produces a blueshift of the excitonic emission lines proportional to ε_{zz} via the deformation potentials.[15,16] The deformation potentials determining the blueshift are not the same for excitons with different symmetries. The X_A and X_B excitons (electron bound to a heavy hole and light hole, respectively) blueshift more rapidly than the X_C exciton (electron bound to a hole from the crystal-field split-off valence band).[15] For a purely uniaxial strain $\varepsilon_{zz}\sim-0.5\%$, the X_A and X_C exciton energies are predicted to cross, so that when $\varepsilon_{zz} > -0.5\%$ the X_C becomes the lowest-lying energy excitonic transition.[16–18]

In this work we study the correlation between the optical and the structural properties of GaN/AlN core-shell NWs, identifying the dependence of the excitonic transitions on the uniaxial strain state. The NWs are grown by plasma-assisted molecular beam epitaxy (PAMBE) on a Si(111) substrate. For shell thickness up to 5 nm, TEM analyses did not reveal any dislocation at the GaN/AlN interface. Both the photoluminescence (PL) of the NW ensembles and the microphotoluminescence (μ-PL) of individual NWs show a progressive blueshift of the emission for increasing shell thickness as a consequence of the increase of the compressive strain in the core. Correlation between the single NW μ-PL and the NW structure analyzed by the HRSTEM established for nine NWs allowed us to directly relate the emission blueshift to the core and shell thicknesses. The results show that the μ-PL energy is a monotonic function of the volume ratio between the GaN core and AlN shell, and that for a strain state $\varepsilon_{zz}^{c} = 0.35\%-0.5\%$ the energies of excitons X_A and X_C cross, in agreement with the elastic theory for purely uniaxial strain.

II. NANOWIRE GROWTH

The samples were grown in a MBE chamber equipped with standard effusion cells for Ga and Al, and a radio-frequency plasma cell to supply active nitrogen. The Si (111) substrates were first etched in 5% HF:H_2O solution for 1 min, rinsed in deionized water, and oxidized under a uv lamp before a second etching process. Prior to the growth, the substrates were thermally cleaned in the growth chamber for 30 min at 850 °C. The growth experiments were monitored by *in situ* reflection high-energy electron diffraction. The growth started with the deposition at 600 °C of Al equivalent to a 2 nm AlN layer thickness onto the Si substrate. Then the sample surface was exposed to the nitrogen plasma for 1 min. After this initial procedure, the substrate temperature was increased to 800 °C and Ga and N were supplied simultaneously to form NWs. We used N-rich growth conditions, obtained with a 2 SCCM (SCCM denotes cubic centimeters per minute at STP) flow of N_2 into a radio-frequency plasma cell powered at 460 W and a Ga flux equivalent to a nominal growth rate of 0.04 nm/s for two-dimensional GaN layers.

These deposition conditions lead to a typical NW elongation rate of 0.07 nm/s in the steady-state regime. The GaN core part was grown for 225 min and the NW synthesis was terminated by the deposition of an AlN cap layer. The same substrate temperature was kept during the AlN deposition. The nominal AlN growth rate was 0.03 nm/s and the Al source axis was tilted at 40° from the substrate normal, so that Al flux could directly impinge the NW sidewalls. This geometry combined with the fact that Al adatoms have a short diffusion length on the nanowire facets result in a significant AlN radial growth, producing core-shell structures.[19] To investigate the effect of the shell thickness on the NW properties, we used different AlN deposition times, varied from 0 to 14 min. After measurement by TEM, the shell thicknesses were found to be consistent with the Al flux impinging the NW facets, i.e., equivalent to a radial growth rate of 0.025 nm/s.

Table I reports the list of the grown samples and their main growth and structural parameters.

III. EXPERIMENTAL TECHNIQUES

Single nanowires from each sample were detached in an ultrasound bath from the Si substrates, and dispersed in ethanol on either Si substrates or C-Formvar TEM membranes supported by Cu square grids with a 50 μm mesh. After dispersion, the NW surface density is in the range of 10^5 cm^{-2} corresponding to 2–5 nanowires per grid square.

Macroscopic PL (macro-PL) on the ensembles and μ-PL on the dispersed nanowires have been performed at $T = 4.2$ K. The samples were cooled down in a continuous-flow liquid He cryostat and excited by means of a frequency-doubled cw Ar^{2+} ion laser at 244 nm. For the μ-PL measurements, the laser was focused on the substrate surface in a spot with a diameter of ~3 μm by means of a uv microscope objective with 0.4 numerical aperture. The excitation power was set in the range 1–100 μW. The lower power limit was used when analyzing single nanowires on C-Formvar membranes in order to avoid any redshift of the PL energy induced by sample heating. The sample was imaged through a uv-sensitive camera in order to visualize the luminescence spot and to locate the nanowire unambiguously for the subsequent HRSTEM analysis. Before HRSTEM, an intermediate transmission-mode scanning electron microscope—field-emission gun–STEM (SEMFEG-STEM) localization step has been performed in order to discard all spectra possibly related to groups of two or more nanowires lying together. For statistical purposes, we analyzed between 20 and 30 single nanowires from each sample. PL spectra were measured using a HR460 spectrometer with a 600 grooves/mm grating and a CCD camera. The energy resolution of the setup during these experiments was in the range of 1 meV.

The crystalline structure of the nine NWs observed by μ-PL was studied by HRSTEM using a TEM-STEM JEOL 2200FS microscope equipped with a Cs-probe aberration corrector. This corrector allows atomic resolution in the bright field and in the *Z*-sensitive high-angle annular dark field (HAADF) STEM imaging modes. NWs were oriented along the $\langle 11\bar{2}0\rangle$ zone axis in order to observe the $\{1\bar{1}00\}$ facets parallel to the viewing direction.

IV. STRUCTURAL PROPERTIES

The bright-field HRSTEM images in Figs. 1(a)—1(f) show different views of a nanowire from sample C. In the images, the nanowire is observed along the $\langle 11\bar{2}0\rangle$ zone axis. This viewing direction is parallel to the NW facets,[20] which is indispensable for accurate imaging of the thin AlN shell region. The GaN core and the AlN shell correspond to the crystalline darker and brighter regions, respectively. The diameter is $d =$ 34.5 nm and the average shell thickness is $\langle t_s\rangle = 1.1$ nm. Some monolayer fluctuations occur along the nanowire body, but the AlN shell is generally homogeneous in thickness. The measurements of the shell thickness are consistent in both bright- and dark-field modes. The images in Figs. 1(e) and 1(f) show that the AlN shell is monocrystalline at the nanowire top as well as at its base. The monocrystallinity of the shell is confirmed in Figs. 1(f)—1(h), showing the top of a nanowire from sample E [Fig. 1(f)] and the two high-resolution details of the core-shell interface [Figs. 1(g) and 1(h). The images also show a residual amorphous layer surrounding the wire, related to the dispersion of NWs in ethanol. This organic layer does not influence the optical or structural properties

TABLE I. Growth and structural parameters of the analyzed samples.

Sample	AlN growth time (min)	GaN growth time (min)	Nanowire height (nm)	Nanowire diameter (nm)
A (reference)				
B	4			
C	8.5	225	300–500	30–60
D	12			
E	14			

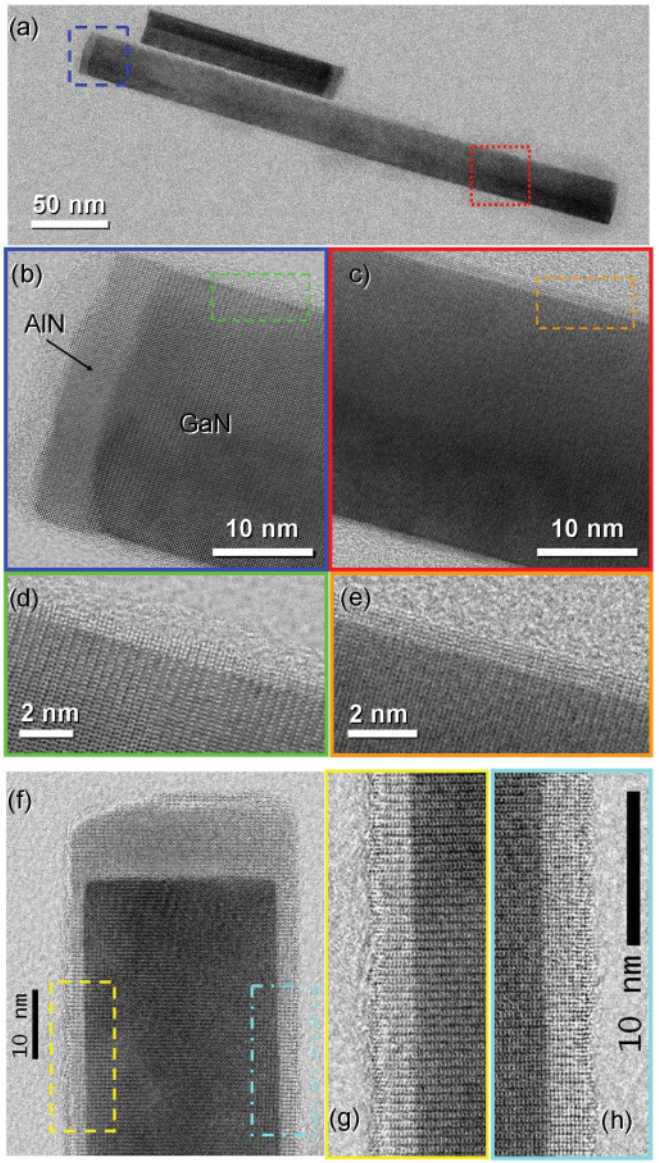

FIG. 1. (Color online) Bright-field HRSTEM images along the $\langle 11\bar{2}0 \rangle$ viewing direction of a nanowire from sample C, showing the GaN core (dark), and the AlN shell (light). (a) View of the whole nanowire; (b) zoom on the nanowire top, identified by the blue dashed rectangle in (a); (c) zoom on the nanowire base, identified by the red dotted rectangle in (a); (d),(e) zooms on the AlN/GaN interface close to the nanowire top and base (identified by the rectangles in (b) and (c), respectively). (f) View of the top of a nanowire from sample E. The average shell thickness is $\langle t_s \rangle = 2.6$ nm; (g),(h) enlargement of the interface regions identified by the left- and right-hand side dashed rectangles in (f). HR observations all along the facets did not reveal any dislocation; the GaN/AlN interface is smooth and the AlN shell is monocrystalline.

of the structure. In sample E, the maximum shell thickness is 5 nm. In all analyzed samples, the nanowires exhibit coherent and atomically sharp AlN/GaN interfaces, with no evidence of dislocations, stacking faults, or compositional intermixing. This was checked by acquiring HRSTEM images along the entire NW length. This picture is consistent with the results previously reported in Ref. 13, which sets the limit for the critical shell thickness for plastic relaxation to beyond 12 nm.

V. OPTICAL PROPERTIES

The results of the PL characterization at T=4.2 K are summarized in Fig. 2. In Fig. 2(a), the macro-PL spectra of the ensembles of samples A (reference GaN sample without AlN shell), C, and E are reported. Figure 2(b) refers to the μ-PL spectra of single nanowires from samples A and E, while in Fig. 2(c) we present the statistics of the μ-PL peak energies. The trends of the ensemble PL peak energy and full width at half maximum (FWHM) as well as of the average μ-PL energy are reported in Fig. 2(d). The macro-PL spectrum of sample

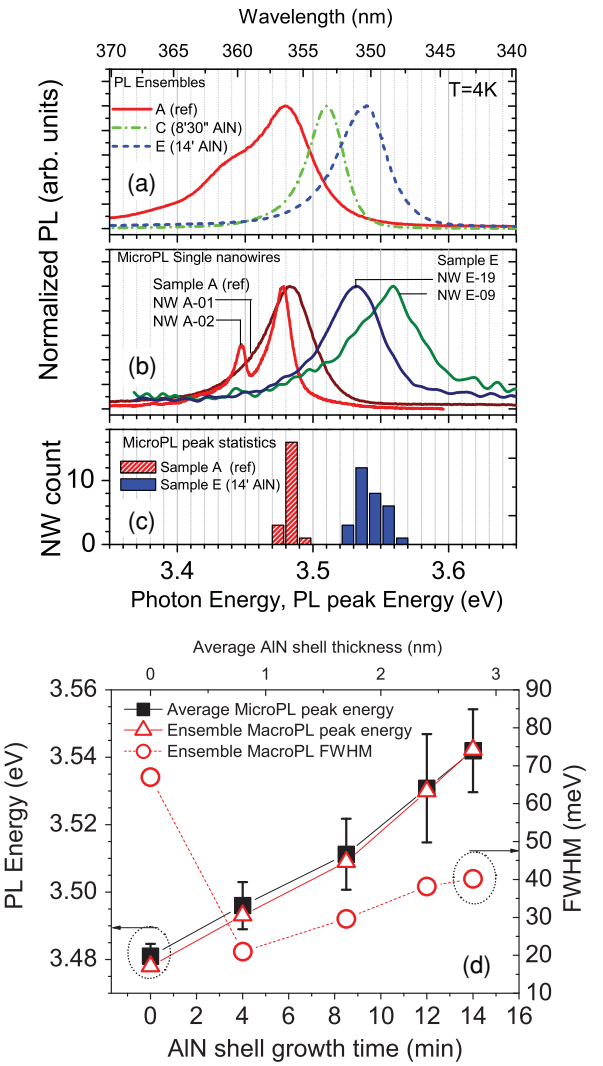

FIG. 2. (Color online) (a) Macro-PL spectra of the ensembles of the reference sample A (solid red line) and of the sample E (14 min AlN shell growth time, dashed blue line) collected at T=4 K. (b) Selected μ-PL spectra collected at T=4 K from single nanowires from samples A and E. (c) Statistics of the μ-PL peak energy of single nanowires from sample A (red patterned bars, statistics from a group of 20 NWs) and sample E (blue bars, statistics from 30 NWs). (d) Dependence of the PL peak energy of the ensembles (red triangles), of the FWHM of the ensemble spectrum (red circles), and of the average PL peak energy (black squares) of single NW spectra on the growth time of the AlN shell. The error bar on this quantity refers to the standard deviation of the statistics realized on 20–30 single NWs per sample. The upper scale is derived from the bottom scale according to the measurements performed by STEM.

A is strongly asymmetric and clearly exhibits the presence of multiple components. The main luminescence peak is at $E = 3.479$ eV, and a shoulder is present at $E \sim 3.45$ eV. The energy of the main peak corresponds to the values reported for the free exciton FX_A (electron bound to a heavy hole[15]) of GaN.[21–25] At low temperature, the X_A exciton may localize on neutral donors (donor-bound exciton D^0X_A), with a localization energy of about 6–7 meV[21,23] and with the same symmetry as the FX_A.[26] It is the dominant luminescence feature in unintentionally doped bulk GaN,[17,23,24] as well as in GaN nanowires.[26–28] In the case of GaN nanowires, the energy of the donor-bound exciton may be blueshifted by several meV because of surface effects.[28] The macro-PL spectra of samples C and E are peaked at $E = 3.510$ eV and $E = 3.541$ eV, respectively. Their shape is much more symmetric than that of sample A. Micro-PL spectra of single nanowires from sample A may show either a single rather broad peak similar to the ensemble luminescence, as in the case of NW A-01, or multiple peaks, as in the case of NW A-02. Based on the statistics performed on 20 nanowires from this sample [Fig. 2(c), the main peak energy is distributed close to the D^0X_A energy. However, other subbandgap peaks may appear, most frequently in the neighborhood of $E = 3.45$ eV. The emission at this energy has been related to an excitonic surface recombination channel whose structure remains unidentified.[27,29] The spectra of single nanowires from sample E present peaks with energies distributed in the interval $E = 3.525$–3.56 eV, in good agreement with the macro-PL from this sample. It should be noted that, in contrast to sample A, none of the spectra from samples B, C, D, and E exhibits multiple emission lines or a substructuration of the main peak.

Figure 2(d) summarizes the dependence of the PL energy and of the spectral width of the analyzed samples on the growth time of the AlN shell. The peak energy of the ensemble $E_{\mathrm{PL}}^{\mathrm{ens}}$, as well as the average energy $\langle E_{\mu-\mathrm{PL}} \rangle$ extracted from the study of 20–30 nanowires per sample, increase with the AlN growth time. This blueshift is expected[15,16] as a consequence of the compression of the GaN core along the z axis by the surrounding AlN shell.[13] Other mechanisms leading to the blueshift of the PL can be excluded. This is the case for increasing n-type doping of the GaN core, because the core of all samples is unintentionally doped and was grown under the same conditions. Band filling effects can also be excluded, since the PL measurements were performed at the same low excitation power in all analyzed samples. The FWHM of the ensemble PL peaks does not increase monotonically: it has the maximum value in the case of the reference sample (no AlN shell), it drops to its minimum for sample B (the thinnest AlN shell), and it then grows monotonically with the AlN growth time. The standard deviation of the μ-PL main peak energy represented as the error bar on the average value of the peak energy also tends to increase with increasing AlN growth time. These observations can be explained as follows. The drop in the FWHM from the reference sample A to the samples with AlN shell is due to the neutralization of surface recombination channels present in the uncapped NWs. In fact, when an AlN shell is present, the chemical nature of the surface states may be modified and the surface-related radiative recombination paths deactivated. This also explains why the emission lines at 3.45 eV characteristic of the GaN surface recombination disappear already in sample B, where the shell thickness is only $t_s \sim 0.7$ nm. The increase in the FWHM with the AlN shell thickness is related to the strain variation arising from the inhomogeneity of the nanowire diameter (see Table I) and of the AlN shell thickness. A thinner shell on a nanowire with larger diameter induces a smaller strain state than a thicker shell on a thinner nanowire. This leads to an enhancement of the broadening of the PL energies as the average shell thickness is increased, because the dispersion of the thickness around its average value increases at the same time.

VI. CORRELATION BETWEEN OPTICAL AND STRUCTURAL PROPERTIES

The direct correlation between the optical and structural properties of the GaN/AlN core-shell nanowire heterostructures has been performed on a subset of the nanowires analyzed by μ-PL. As this method is extremely time consuming, we limited our analysis to a set of nine nanowires from samples C and E, carefully selected in order to cover the largest possible interval of μ-PL peak energies. Figures 3(a) and 3(b) show the STEM images of nanowires E-09 and E-19, whose spectra can be found in Fig. 2(b). The two nanowires, though originating from the same sample, present significant structural differences. In nanowire E-09 [Fig. 3(b), the diameter is $d = 32.2$ nm but the shell thickness is not uniform. ($t_1 = 2.7$ nm, on the left-hand side, $t_2 = 4.3$ nm on the right-hand side). This nonuniformity of the shell thickness explains the bending of the nanowire, because the GaN core is more compressed on the side with the thicker shell. In nanowire E-19, the volume of the GaN part is more important, the diameter being $d = 53.2$ nm, and the shell thickness being $t_1 = t_2 = 2.7$ nm, uniform within the measurement uncertainty. This example shows that the μ-PL peak energy significantly changes with the $V_{\mathrm{AlN}}/V_{\mathrm{GaN}}$ ratio. It also shows that nonuniform shells induce a bending of the NW axe. Only two out of the nine analyzed nanowires were bent because of a nonuniform shell thickness. In these cases, the PL spectrum exhibits an asymmetric shape compared to the case of NWs with uniform shell. These results suggest a correlation between the geometrical symmetry of the wire and the symmetry of its μ-PL spectrum.

In coherent nanowire core-shell heterostructures with uniform shell thickness, it has been shown in previous works that the contribution of the in-plane component is much lower than that of the axial one, $\varepsilon_{xx} + \varepsilon_{yy} \ll \varepsilon_{zz}$. For instance, in the case of a nanowire with a core radius $R_c = 25$ nm and a shell thickness $t_s = 2$ nm, the VFF calculations yield for the GaN core an on-axis strain $\varepsilon_{zz} = -0.55\%$, and an in-plane strain $\varepsilon_{xx} + \varepsilon_{yy} = -0.021\%$. For this reason, it is possible to express the strain ε_{zz}^{c} component in the GaN core as an analytic function of the nanowire structural parameters:[13]

$$\varepsilon_{zz}^{c} = \frac{F}{1+F} \frac{c_0^{\mathrm{AlN}} - c_0^{\mathrm{GaN}}}{c_0^{\mathrm{GaN}}}, \tag{1a}$$

where

$$F = \frac{V_{\mathrm{AlN}}}{V_{\mathrm{GaN}}} \frac{c_{33}^{\mathrm{AlN}}}{c_{33}^{\mathrm{GaN}}} \left(\frac{c_0^{\mathrm{GaN}}}{c_0^{\mathrm{AlN}}} \right)^2 = \frac{t_s^2 + 2R_c t_s}{R_C^2} \frac{c_{33}^{\mathrm{AlN}}}{c_{33}^{\mathrm{GaN}}} \left(\frac{c_0^{\mathrm{GaN}}}{c_0^{\mathrm{AlN}}} \right)^2. \tag{1b}$$

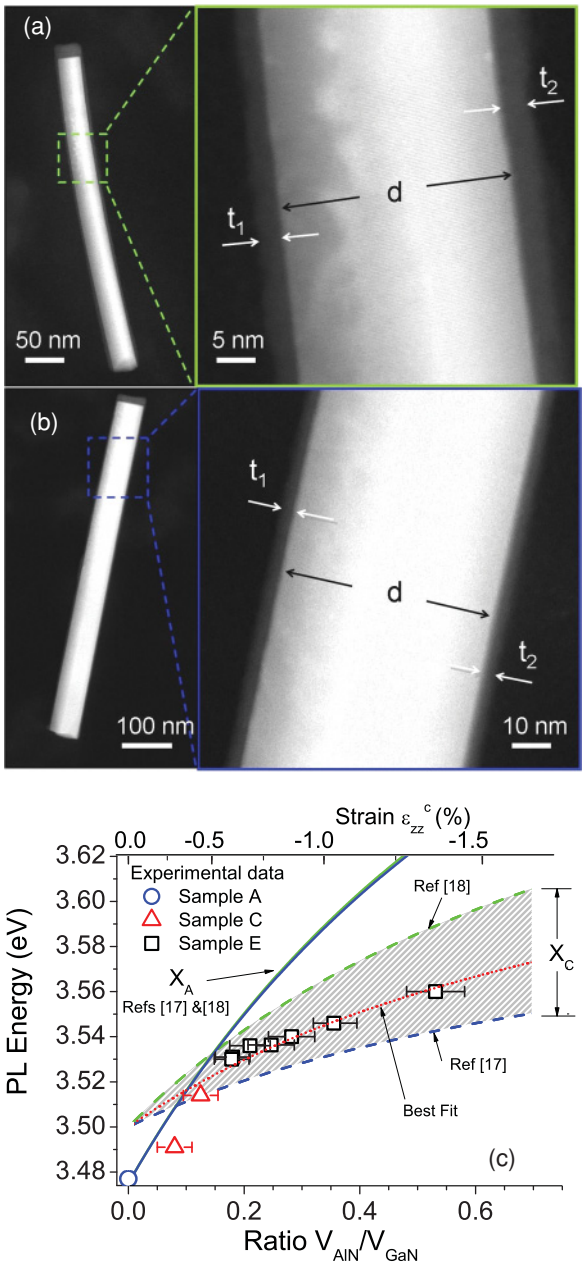

FIG. 3. (Color online) Correlation between μ-PL and HRSTEM data. (a),(b) STEM-HAADF analysis of the nanowires E-09 (a) and E-19 (b) from sample E. The images show the whole NW (left) and a detail of the same nanowire (right). t_1, t_2, and d refer to the shell thicknesses and to the NW diameter, respectively. (c) Correlation between the volume ratio of AlN to GaN and the μ-PL peak energy measured for ten NWs from samples A, C, and E. Solid and dashed lines refer to the predictions of the dependence of the exciton energy on the volume ratio $V_{\mathrm{AlN}}/V_{\mathrm{GaN}}$ for the excitons X_A and X_C, respectively, calculated according to Eqs. (1)—(3). The upper and lower limits of the theoretical predictions are determined by using the values of the deformation potentials reported in Refs 17 (blue lines) and 18 (green lines), respectively. The red dotted line is the best fit of our data for the dependence of the X_C exciton. The upper abscissa scale is derived from the lower one according to Eq. (1).

Here $c_{33}^{\mathrm{GaN,AlN}}$ are the macroscopic elastic constants in the core and shell, respectively, and $c_0^{\mathrm{GaN,AlN}}$ are the unstrained lattice constants along the z axis for GaN and AlN. For the GaN/AlN heterostructure system, therefore, the strain state only depends on the volumetric ratio $V_{\mathrm{AlN}}/V_{\mathrm{GaN}}$. We have verified these conclusions by performing calculations within the finite-element model implemented by the strain solver of the commercial software NEXTNANO^3.[30] Our calculations agree with those in Ref. 13, with only a slight difference for the in-plane strain. For the above-mentioned example of a NW with $R_c = 25$ nm and $t_s = 2$ nm we calculated $\varepsilon_{xx}+\varepsilon_{yy} = -0.031\%$, still much lower than the on-axis component. As the length of the nanowire is much larger than the AlN cap thickness, the latter can be neglected in the calculations. Given these assumptions, it is then straightforward to establish the relationship between the geometrical parameters of the nanowire and the PL energy of the exciton types involved in the transitions, which is a linear function of ε_{zz}^c:[15–17]

$$E_{A,B}\left(\varepsilon_{zz}^c\right) = E_{A,B}(0) + [a_{cz} - D_1 - D_3]\varepsilon_{zz}^c, \quad (2)$$

$$E_C\left(\varepsilon_{zz}^c\right) = E_C(0) + [a_{cz} - D_1]\varepsilon_{zz}^c, \quad (3)$$

where Eq. (2) refers to type A and B excitons (electrons bound with heavy and light holes, respectively), and Eq. (3) to type C excitons (electrons bound with split-off holes). The quantities a_{cz}, D_1, and D_3 are the GaN conduction and valence band deformation potentials involved in the band shift under uniaxial strain on the z axis.[15,16]

Figure 3(c) shows the results of the correlation between the HRSTEM and the μ-PL of the nanowires. The PL energy of the nanowire is plotted as a function of the volumetric ratio $V_{\mathrm{AlN}}/V_{\mathrm{GaN}}$. This ratio has been determined from the STEM measurements. In the case of asymmetric nanowires, we assumed an effective shell thickness t_s^{eff} equal to the minimum shell thickness measured. This assumption is justified by the fact that the crystal is less compressed on the nanowire side with the minimal shell thickness. Therefore, excitons will tend to recombine on this side of the nanowire, where the recombination energy is minimal. The upper abscissa scale in the plot of Fig. 3(c) refers to the effective strain in the GaN core as deduced from Eq. (1a).

The experimental results have been compared with the theoretical predictions according to Eqs. (1)–(3). It is important to notice that the predictions strongly depend on the choice of the relevant parameters among the values reported in the literature. These values can be significantly different, especially in the case of the deformation potentials. Therefore, we chose to compare our data with the predictions according to the values proposed by Ghosh *et al.*[17] and by Ishii *et al.*,[18] which provide a lower[17] and upper[18] limit to the value of the calculated PL energy as a function of the ratio $V_{\mathrm{AlN}}/V_{\mathrm{GaN}}$. The values of the deformation potentials and of the other material parameters appearing in Eqs. (1)–(3) are reported in Table II. The calculations predict the crossing of X_A and X_C excitons for a $V_{\mathrm{AlN}}/V_{\mathrm{GaN}}$ ratio of 0.1–0.15. The observed dependence of the μ-PL energy on the volumetric ratio $V_{\mathrm{AlN}}/V_{\mathrm{GaN}}$ is in good agreement with the theory. In particular, we can clearly identify the crossing of the different exciton types X_A and X_C. In fact, for $V_{\mathrm{AlN}}/V_{\mathrm{GaN}} \leqslant 0.1$ and $\varepsilon_{zz}^c \geqslant -0.35\%$, E_{PL} matches fairly well with the prediction for the X_A exciton, while for $V_{\mathrm{AlN}}/V_{\mathrm{GaN}} \geqslant 0.15$ and $\varepsilon_{zz}^c \leqslant -0.5\%$ it strongly deviates from

TABLE II. Material parameters.

	AlN	GaN	
z-axis lattice constant c_0 (Å)	4.982	5.185	
Elastic constant c_{33} (GPa)	373	398	
Deformation potentials for GaN	Ref. 17	Ref. 18	This work
$a_{cz}-D_1$ (eV)	−3.1	−6.5	−4.5
D_3 (eV)	8.2	4.9	
Unstrained GaN exciton energies	Ref. 25		
$E_A(0)$ (eV)	3.478		
$E_C(0)$ (eV)	3.50		

the behavior of the X_A exciton and follows the predictions for the X_C exciton. All points relative to the analyzed nanowires lie between the predictions by the two above-cited references, which confirms the theoretical prediction of the X_A and X_C exciton energy crossing. Keeping the zero-strain X_C energy as fixed, the best fit of the X_C energy as a function of the strain state is obtained in the present measurement for a deformation potential $a_{cz}-D_1 = -4.5$ eV.

VII. CONCLUSIONS

In conclusion, we have studied the optical properties of GaN/AlN core-shell heterostructures grown by PAMBE on a Si(111) substrate. The heterostructure interfaces are free of dislocations, as shown by the HRSTEM analysis. The AlN shell induces a uniaxial and uniform compression of the GaN core along the nanowire axis. Both the PL of the NW ensembles and the μ-PL of individual NWs show a progressive blueshift of the emission for increasing shell thickness as a consequence of the increase of the compressive strain in the core. Moreover, the AlN shell efficiently passivates the surface-related luminescence found in the uncapped nanowires at $E_{\mathrm{ph}} = 3.45$ eV. By means of correlated μ-PL and HRSTEM measurements performed on a set of nine NWs, we directly related the emission blueshift to the core and shell thicknesses. The results show that the μ-PL energy is a monotonic function of the volume ratio between GaN core and AlN shell. Moreover, we evidenced that for a strain state $\varepsilon_{zz}^{c} = 0.35\% - -0.5\%$ the excitons X_A and X_C cross, as predicted by the elastic theory for purely uniaxial strain.

ACKNOWLEDGMENTS

We gratefully acknowledge Y. M. Niquet for fruitful discussion on the strain relaxation in nanowire core-shell structures. This work was supported by the French ANR agency under Programs No. ANR-08-NANO-031 BoNaFo and No. ANR-08-BLAN-0179 NanoPhotoNit.

*Corresponding author: lorenzo.rigutti@ief.u-psud.fr

[1] F. Qian, S. Gradecak, Y. Li, C.-Y. Wen and C. M. Lieber, Nano Lett. **5**, 2287 (2005).
[2] S. Gradecak, F. Qian, Y. Li, H.-G. Park, and C. M. Lieber, Appl. Phys. Lett. **87**, 173111 (2005).
[3] Y. Dong, B. Tian, T. J. Kempa and C. M. Lieber, Nano Lett. **9**, 2183 (2009).
[4] L.-F. Cui, R. Ruffo, C. K. Chan, Hailin Peng, and Y. Cui, Nano Lett. **9**, 491 (2009).
[5] J. W. W. van Tilburg *et al.*, Semicond. Sci. Technol. **25,** 024011 (2010).
[6] O. Demichel, F. Oehler, P. Noe, V. Calvo, N. Pauc, P. Gentile, T. Baron, D. Peyrade, and N. Magnea, Appl. Phys. Lett. **93**, 213104 (2008).
[7] F. Fabbri, F. Rossi, G. Attolini, G. Salviati, S. Iannotta, L. Aversa, R. Verucchi, M. Nardi, N. Fukata, B. Dierre, and T. Sekiguchi, Nanotechnology **21,** 345702 (2010).
[8] C. M. Warwick and T. W. Clyne, J. Mater. Sci. **26**, 3817 (1991).
[9] M. Y. Gutkin, I. A. Ovid'ko, and A. G. Sheinerman, J. Phys.: Condens. Matter **12**, 5391 (2000).
[10] T. E. Trammell, X. Zhang, Y. Li, L. Q. Chen, and E. C. Dickey, J. Cryst. Growth **310**, 3084 (2008).
[11] S. Raychaudhuri and E. T. Yu, J. Appl. Phys. **99**, 114308 (2006).
[12] J. Grønqvist, N. Sondergaard, F. Boxberg, Th. Guhr, S. Aberg, and H. Q. Xu, J. Appl. Phys. **106**, 053508 (2009).
[13] K. Hestroffer, R. Mata, D. Camacho, C. Leclere, G. Tourbot, Y. M. Niquet, A. Cros, C. Bougerol, H. Renevier, and B. Daudin Nanotechnology **21,** 415702 (2010).
[14] D. Camacho and Y. M. Niquet, Physica E **42**, 1361 (2010).
[15] S. L. Chuang and C. S. Chang, Phys. Rev. B **54**, 2491 (1996).
[16] Q. Yan, P. Rinke, M. Scheffler, and C. G. Van de Walle, Appl. Phys. Lett. **95**, 121111 (2009).
[17] S. Ghosh, P. Waltereit, O. Brandt, H. T. Grahn, and K. H. Ploog, Phys. Rev. B **65**, 075202 (2002).
[18] R. Ishii, A. Kaneta, M. Funato, Y. Kawakami, and A. A. Yamaguchi, Phys. Rev. B **81**, 155202 (2010).
[19] M. Tchernycheva, C. Sartel, G. Cirlin, L. Travers, G. Patriarche, J.-C. Harmand, Le Si Dang, J. Renard, B. Gayral, L. Nevou, and F. H. Julien, Nanotechnology **18,** 385306 (2007).
[20] L. Largeau, D. L. Dheeraj, M. Tchernycheva, G. E. Cirlin, and J. C. Harmand, Nanotechnology **19,** 155704 (2008).
[21] B. Monemar, Phys. Rev. B **10**, 676 (1974).
[22] G. D. Chen, M. Smith, J. Y. Lin, H. X. Jiang, Su-Huai Wei, M. Asif Khan, and C. J. Sun, Appl. Phys. Lett. **68**, 2784 (1996).
[23] K. Kornitzer, T. Ebner, K. Thonke, R. Sauer, C. Kirchner, V. Schwegler, M. Kamp, M. Leszczynski, I. Grzegory, and S. Porowski Phys. Rev. B **60**, 1471 (1999).
[24] A. Wysmolek, K. P. Korona, R. Stępniewski, J. M. Baranowski, J. Błoniarz, M. Potemski, R. L. Jones, D. C. Look, J. Kuhl, S. S. Park, and S. K. Lee, Phys. Rev. B **66**, 245317 (2002).
[25] I. Vurgaftman and J. R. Meyer, J. Appl. Phys. **94,** 3675 (2003).
[26] J. B. Schlager, N. A. Sanford, K. A. Bertness, J. M. Barker, A. Roshko, and P. T. Blanchard, Appl. Phys. Lett. **88,** 213106 (2006).

[27]F. Furtmayr, M. Vielemeyer, M. Stutzmann, A. Laufer, B. K. Meyer, and M. Eickhoff, J. Appl. Phys. **104**, 074309 (2008).

[28]O. Brandt, C. Pfüller, C. Chèze, L. Geelhaar, and H. Riechert Phys. Rev. B **81**, 045302 (2010).

[29]E. Calleja, M. A. Sanchez-Garcia, F. J. Sanchez, F. Calle, F. B. Naranjo, E. Munoz, U. Jahn, and K. Ploog, Phys. Rev. B **62**, 16826 (2000).

[30]See NEXTNANO website [http://www.wsi.tum.de/nextnano3] for detailed documentation.